ORIGINAL ARTICLE

Journal of Cachexia, Sarcopenia and Muscle 2018; **9**: 71–85
Published online 19 November 2017 in Wiley Online Library (wileyonlinelibrary.com) **DOI:** 10.1002/jcsm.12246

Serum and urine metabolomics study reveals a distinct diagnostic model for cancer cachexia

Quan-Jun Yang[1†], Jiang-Rong Zhao[2†], Juan Hao[2†], Bin Li[1,3], Yan Huo[1], Yong-Long Han[1], Li-Li Wan[1], Jie Li[1], Jinlu Huang[1], Jin Lu[1], Gen-Jin Yang[4*] & Cheng Guo[1*]

[1]*Department of Pharmacy, Shanghai Jiao Tong University Affiliated Sixth People's Hospital, Shanghai 200233, China;* [2]*Department of Gastroenterology, Shanghai Traditional Chinese Medicine-Integrated Hospital, Shanghai University of Traditional Chinese Medicine, Shanghai, China;* [3]*Department of Medical Oncology, Benxi Center Hospital, Benxi 117000, China;* [4]*School of Pharmacy, Second Military Medical University, Shanghai 200433, China*

Abstract

Background Cachexia is a multifactorial metabolic syndrome with high morbidity and mortality in patients with advanced cancer. The diagnosis of cancer cachexia depends on objective measures of clinical symptoms and a history of weight loss, which lag behind disease progression and have limited utility for the early diagnosis of cancer cachexia. In this study, we performed a nuclear magnetic resonance-based metabolomics analysis to reveal the metabolic profile of cancer cachexia and establish a diagnostic model.

Methods Eighty-four cancer cachexia patients, 33 pre-cachectic patients, 105 weight-stable cancer patients, and 74 healthy controls were included in the training and validation sets. Comparative analysis was used to elucidate the distinct metabolites of cancer cachexia, while metabolic pathway analysis was employed to elucidate reprogramming pathways. Random forest, logistic regression, and receiver operating characteristic analyses were used to select and validate the biomarker metabolites and establish a diagnostic model.

Results Forty-six cancer cachexia patients, 22 pre-cachectic patients, 68 weight-stable cancer patients, and 48 healthy controls were included in the training set, and 38 cancer cachexia patients, 11 pre-cachectic patients, 37 weight-stable cancer patients, and 26 healthy controls were included in the validation set. All four groups were age-matched and sex-matched in the training set. Metabolomics analysis showed a clear separation of the four groups. Overall, 45 metabolites and 18 metabolic pathways were associated with cancer cachexia. Using random forest analysis, 15 of these metabolites were identified as highly discriminating between disease states. Logistic regression and receiver operating characteristic analyses were used to create a distinct diagnostic model with an area under the curve of 0.991 based on three metabolites. The diagnostic equation was Logit(P) = −400.53 − 481.88 × log(Carnosine) −239.02 × log(Leucine) + 383.92 × log(Phenyl acetate), and the result showed 94.64% accuracy in the validation set.

Conclusions This metabolomics study revealed a distinct metabolic profile of cancer cachexia and established and validated a diagnostic model. This research provided a feasible diagnostic tool for identifying at-risk populations through the detection of serum metabolites.

Keywords Cancer cachexia; Metabolomics; Logistic regression; Biomarker; Leucine

Received: 28 March 2017; Revised: 3 August 2017; Accepted: 11 August 2017
**Correspondence to:* Cheng Guo, Shanghai Jiao Tong University Affiliated Sixth People's Hospital, No. 600, Road Yishan, Shanghai 200233, China. Tel: +86 21 24058098, Email: guopharm@126.com; Gen-Jin Yang, School of Pharmacy, Second Military Medical University, Shanghai 200433, China. Email: gjinyang@hotmail.com
†Contributed equally to this work

Introduction

Although the overall prognosis of cancer patients has improved since the early 1990s, the 5 year survival rate of cancer patients remains low.[1,2] Cachexia is thought to be the main cause of death in cancer patients, and its morbidity and mortality are high without effective treatment.[3,4] This condition occurs in nearly 80% of patients with advanced cancer

and contributes to approximately 30% of cancer mortality.[5] It is associated with a reduced quality of life, reduced therapy response, and reduced treatment tolerance.[2,6] Recent clinical and experimental evidence clearly indicates that cancer cachexia is not an ineluctable occurrence,[1,7–9] and an international consensus on the definition of cancer cachexia has been reached.[10] However, there is no molecular biomarker with high sensitivity and specificity that can be employed for the early and accurate diagnosis of cancer cachexia.

Cancer cachexia is characterized by weight loss, adipose tissue wasting, muscle atrophy, and loss of appetite.[11] A clinical diagnosis of cachexia requires patient weight-loss history and may be severely underestimated. As cachexia can develop progressively through various stages, from pre-cachexia to cachexia to refractory cachexia, early screening and staging is particularly important to prevent or delay the onset of cachexia.[10] Consistent with its biochemical and molecular mechanisms, cachexia involves the secretion of tumour-derived catabolic factors and host-derived proinflammatory cytokines.[12] These catabolic factors and cytokines lead to changes in host metabolism and energy expenditure. Glucocorticoid abnormalities and insulin resistance are also often present in cancer patients and animal models of cancer cachexia.[13–15] These metabolic disorders not only potentially underlie the pathogenesis of weight loss but also result in multiple and severe consequences, ranging from impairment of immune function to poor outcome to chemotherapy, fatigue, muscle weakness, and markedly reduced quality of life.[12,16] Moreover, metabolic dysfunction occurs before weight loss and muscle atrophy.[17,18] Hence, metabolite changes have been hypothesized as biomarkers for the diagnosis of cachexia.

Previous studies have shown an association between cancer cachexia and hypoglycaemia, hyperlipidaemia, and decreasing levels of branched-chain amino acids.[17–19] However, these biomarkers have poor sensitivity and specificity. Our previous studies of animal models revealed the dynamically changing metabolic profile of cancer cachexia and identified the involvement of five metabolic pathways, including low blood glucose, elevated ketone bodies, decreased branched-chain amino acids, increased neutral amino acids, and high levels of 3-methylhistidine and creatine.[20–22] To validate these results, a serum and urine metabolomics approach was employed to reveal the metabolic profile of cancer cachexia and establish a diagnostic model for cancer cachexia.

Materials and methods

Patient selection

Ethics approval was obtained from the Health Research Ethics Board at Shanghai Jiao Tong University Affiliated Sixth People's Hospital. Patients were recruited between July 2013 and February 2017 at Shanghai Jiao Tong University Affiliated Sixth People's Hospital (n = 48), Shanghai Traditional Chinese Medicine-Integrated Hospital, Shanghai University of Traditional Chinese Medicine (n = 68), and First People's Hospital of Benxi (n = 68). All participants provided written informed consent. Based on the diagnostic criteria from the international consensus,[10] we recruited cancer-cachexic patients, pre-cachectic patients, weight-stable cancer patients, and weight-stable healthy controls. Groups were matched by age, gender, and primary cancer type. Cancer cachexia was recognized in individuals as follows: weight loss $>$5% in the past 6 months or weight loss $>$2% in the past 6 months and a body mass index (BMI) $<$20 kg/m^2. Pre-cachexia was recognized as weight loss $<$5% in the past 6 months and a BMI $>$20 kg/m2. Weight-stable cancer patients were considered to include those with a BMI $<$25 kg/m^2 and no marked weight change during the previous year. The weight-stable healthy controls were recruited from among healthy subjects during an annual wellness visit. Age, height, weight, cancer biomarkers, and biochemical biomarkers were obtained from patient laboratory reports, either from the date of diagnosis or from the date closest to diagnosis. Exclusion criteria were as follows: chemotherapy near the time of sample acquisition, kidney or liver failure, acquired immunodeficiency syndrome, inflammatory bowel disease, and systemic infection. Primary cancer types included lung cancer, liver cancer, colorectal cancer, gastric cancer, cardiac cancer, renal cancer, breast cancer, oesophageal cancer, and pancreatic cancer. To identify the metabolic profile and establish a diagnostic model of cancer cachexia, independent serum and urine samples were collected to generate a validation set during the period from January 2015 to February 2017. Sample collection and inclusion and exclusion criteria were the same as for the training sets. Table 1 shows the general characteristics of the patients in each group.

Sample collection

Morning fasting blood was collected in a Vacutainer tube, and the last morning urine was collected midstream in a urine tube. The blood samples were kept at room temperature for 30 min for clotting. Clotted blood samples were centrifuged at 3000 × g at 4°C for 20 min to remove the supernatant serum and quickly stored at −80°C until the ^{1}H nuclear magnetic resonance (NMR) analysis was conducted. Within 2 h of the urine sample collection, each mL of urine was mixed with 50 μL of 0.42% sodium azide preservative. The pH of urine was adjusted to 7.0 with 1M Tris-HCl (pH 7.0) and biobanked at −80°C. To ensure robust and reproducible data, all the samples were prepared according to the Bruker protocol.[23] Briefly, the samples were thawed at 4°C for 2 h and left at room temperature for 1 h. Thereafter, 300 μL thawed samples were mixed with 300 μL of phosphate buffer (pH 7.4)

Table 1 Demographic and cancer biomarker characteristics of patients and controls.

	Training set (N = 184)				Validation set (N = 112)			
	Cachexia (N = 46)	Pre-cachexia (N = 22)	Cancer (N = 68)	Control (N = 48)	Cachexia (N = 38)	Pre-cachexia (N = 11)	Cancer (N = 37)	Control (N = 26)
Age (years) (median, range)	70, 52–78	73, 57–84	66, 48–89	65, 50–71	74, 54–87[*#]	72, 56–81	64, 61–89	66, 48–72
Male/female	22/24	10/12	36/32	22/26	19/19	5/6	17/20	12/14
Cancer types[f]								
Lung cancer	7(15.22)	2(9.09)	13(19.12)	—	5(13.16)	2(18.18)	13(35.14)	/
Liver cancer	14(30.43)	7(31.82)	14(20.59)	—	6(15.79)	3(27.27)	11(29.73)	/
Colorectal cancer	4(8.7)	2(9.09)	8(11.76)	—	3(7.89)	2(18.18)	2(5.41)	/
Gastric cancer	9(19.57)	3(13.64)	11(16.18)	—	12(31.58)	1(9.09)	4(10.81)	/
Cardiac cancer	1(2.17)	-	2(2.94)	—	1(2.63)	—	—	/
Renal cancer	1(2.17)	2(9.09)	4(5.88)	—	-	—	2(5.41)	/
Breast cancer	2(4.35)	3(13.64)	10(14.71)	—	3(7.89)	—	4(10.81)	/
Oesophageal cancer	1(2.17)	1(4.55)	4(5.88)	—	—	—	1(2.7)	/
Pancreatic cancer	7(15.22)	2(9.09)	2(2.94)	—	8(21.05)	3(27.27)	—	/
Cancer markers								
α-Fetoprotein (ng/mL)	173.61 ± 300.51[a]	201.54 ± 259.84[ab]	43.55 ± 116.43		176.08 ± 455.92[a]	126.54 ± 163.62[abd]	63.3 ± 82.03[e]	
Carcinoembryonic antigen (ng/mL)	51.97 ± 181.96[a]	42.56 ± 72.54[ab]	16.34 ± 5.92		26.44 ± 48.03[ac]	15.68 ± 48.70[abd]	7.72 ± 8.10[e]	
Carbohydrate antigen 19–9 (U/mL)	317.58 ± 407.94[a]	254.50 ± 114.75[ab]	55.74 ± 60.59		125.09 ± 222.77[ac]	216.28 ± 175.81[abd]	50.15 ± 58.28	
Carbohydrate antigen 72–4 (U/mL)	37.56 ± 71.61[a]	18.54 ± 17.62[ab]	2.41 ± 1.99		12.24 ± 28.21[ac]	12.06 ± 21.76[ad]	4.79 ± 5.00[e]	
Carbohydrate antigen 12–5 (U/mL)	195.64 ± 278.55 [a]	176.54 ± 157.45 [a]	41.22 ± 58.39		274.83 ± 590.37[ac]	110.44 ± 220.81 [abd]	65.79 ± 99.59[e]	
Carbohydrate antigen 15–3 (U/mL)	22.41 ± 26.41 [a]	22.58 ± 18.64 [a]	7.81 ± 2.82		25.33 ± 32.42[a]	21.96 ± 31.78 [a]	11.33 ± 8.69[e]	
Carbohydrate antigen 242 (IU/mL)	49.56 ± 75.52 [a]	35.61 ± 44.81 [ab]	24.74 ± 33.24		31.42 ± 30.85[ac]	25.63 ± 88.79 [ab]	19.29 ± 29.25	
Carbohydrate antigen 50 (IU/mL)	201.54 ± 189.63 [a]	61.55 ± 48.95 [ab]	40.16 ± 39.19		114.61 ± 161.34[ac]	131.86 ± 74.54 [abd]	103.01 ± 157.88[e]	
Cytokeratin 19 fragments (ng/mL)	11.96 ± 24.66 [a]	9.87 ± 10.19 [ab]	3.12 ± 2.23		25.65 ± 77.88[ac]	32.49 ± 41.66 [abd]	19.66 ± 44.33[e]	
Procalcitonin (ng/mL)	0.87 ± 2.04 [a]	0.38 ± 0.62 [ab]	0.24 ± 0.16		0.42 ± 0.91[ac]	0.18 ± 1.20 [bd]	0.19 ± 0.16	
α-L-fucosidase (U/L)	44.95 ± 18.64 [a]	35.57 ± 42.52 [ab]	29.67 ± 7.89		32.55 ± 9.87[ac]	47.19 ± 57.11 [abd]	36.41 ± 14.48[e]	
Interleukin-6 (pg/mL)	94.63 ± 34.58 [a]	81.69 ± 87.52[a]	48.61 ± 43.47		78.67 ± 39.57[a]	63.53 ± 79.89 [abd]	40.22 ± 47.21	

[a]Significant difference between cancer patients in the same set.
[b]Significant difference between pre-cachexia and cachexia patients in the same set.
[c]Significant difference between cachexia patients in the training set.
[d]Significant difference between pre-cachectic patients in the training set.
[e]Significant difference between cancer patients in the training set.
[f]The number and percentage of each cancer type are listed as N(%).

containing 10% of D_2O. After vortex mixing and centrifugation, 550 μL of the solution were transferred into 5 mm NMR tubes and kept at 4°C until the NMR analysis.

Collection of cancer biomarker and routine biochemical analysis report

Clinical routine biochemistry tests and circulating tumour biomarker measurements were performed according to the manufacturer's protocol by the hospital laboratory. The results of the collected data were verified and recorded. The assays for these biomarkers have demonstrated satisfactory performance and reproducibility except for interleukin-6. Repeated measurement was obtained for interleukin-6 using a high-sensitivity chemiluminescent assay (R&D Systems, Minneapolis, MN, USA). All the samples were assayed in duplicate and averaged to calculate the concentrations in the same analytic batch.

^{1}H-NMR spectroscopy

All spectra were recorded using a Bruker AMX-600 NMR (Bruker, Rheinstetten, Germany) spectrometer that was operated at a 600.13 MHz ^{1}H resonance frequency. Quality control tests were performed at the beginning of every measurement day. A representative sample was used for NMR probe tuning and matching, determination of the transmitter offset value for water-pulse pre-saturation, and 90 pulse adjustments. Each sample was locked and shimmed automatically; receiver gain was set to 90.5 and temperature to 310 K for all experiments. All spectra were acquired and performed using TopSpin software package version 3.0 (Bruker Biospin, Rheinstetten, Germany). The NMR spectroscopy of urine samples was collected with a pre-saturation ^{1}H - NOESY pulse sequence (equation as relaxation delay -90° - t1-90° - tm-90° acquisition, where the relaxation delay was 2 s, t1 was 4 μs, and tm was 100 ms). A total of 128 scans with a spectral width of 5 kHz was collected for all NMR spectra. All the signals were zero filled to 32 k before Fourier transformation. The NMR spectroscopy of serum samples was collected with Carr–Purcell–Meiboom–Gill (CPMG) pulse sequence (equation as relaxation delay -90°-(t-180°-t) n - acquisition, where the relaxation delay was 2 s, t was 400 μs).

Metabolite identification and chemical signal assignment

Chenomx NMR Suite software version 8.1 (Chenomx, Inc., Alberta, Canada) was used for the identification of metabolites in the ^{1}H-NMR spectra of biological samples. Owing to the overlap of signals in the ^{1}H-NMR spectrum, two-dimensional (2D) J-resolved and heteronuclear single bond coherence (HSQC) spectra were used for metabolite identification and signal assignment. 2D J-resolved spectra were acquired using 16 transients per increment for a total of 32 increments that were collected into 16 k data points with spectral widths of 6 kHz along the direct chemical shift axis and 50 Hz along the spin–spin coupling axis. Prior to Fourier transformation, datasets were zero-filled to 128 points in the spin–spin coupling axis and 32 768 points in the chemical shift axis. HSQC spectra can provide excellent spectral dispersion along the indirect ^{13}C dimension and allow the separation of many of the peaks that overlap in a 1D NMR spectrum.

Statistical analysis

NMR data reduction

After the Fourier transformation, phase correction and baseline correction were carefully performed. The ^{1}H chemical shifts referred to the methyl doublet signal of lactate (δ1.33). The corrected NMR spectra, corresponding to the chemical shift range of δ 0.2–10.0, were imported into AMIX 3.9.5 (Bruker Biospin, Rheinstetten, Germany), and all the spectra were reduced into integral regions of equal lengths of 0.005 p.p.m. Regions of δ 4.7–5.1 that contained the resonance from residual water were set to zero. To reduce the concentration differences between the samples, the data were normalized to the total spectral area (100%).

Metabolomics analysis

The dataset was analysed with pattern-recognition methods using the software package Simca version 14.1 (UmetricsAB, Umeå, Sweden). The response variables were centred and scaled to Pareto variance, and the base weight was computed as 1/squareroot (standard deviation of the response variables). Moreover, to normalize the skewed distributions, log transformations were used for non-linear conversions of the data. To eliminate the effect of inter-subject variability and to identify endogenous metabolites that contributed significantly to the classification, linear combinations of X variables orthogonal to the Y vector were removed by orthogonal projections to latent structures (OPLS)-discriminant analysis (DA).[24,25]

Metabolic network analysis

To identify the most relevant metabolic pathways in cancer cachexia, pathway analysis was used for pathway-enrichment analysis and pathway-topology analysis. The metabolites with variable importance in the projection (VIP) scores >1.0 in PLS or p1 $\geq \pm$ 0.05 in S-Plot were examined and selected for discrimination power according to multiple statistical criteria. GlobalTest was used to analyse the concentration values and identify subtle changes, and a relative-betweenness centrality was used to establish metabolite importance.

Selection of biomarker candidates

Establishing a diagnostic model to predict the presence of cachexia through the distinct metabolic profile was difficult because of the high-dimensional dataset. To improve the prediction of cachexia, random forest analysis was performed to determine whether the metabolic data could successfully differentiate the four groups. Then, a forward stepwise logistic regression model was constructed on the training sample set to design the best metabolite combination. Receiver Operating Characteristic (ROC) curves were used to evaluate the accuracy of this model in the validation sets following the DeLong method. The global performance of each biomarker model was evaluated using the Area Under the Curve (AUC) and the determination of sensitivity and specificity at the optimal cut-off point defined by the minimum distance to the top-left corner.

General statistical analysis

Data entry and analysis were performed with MedCalc software version 13.0.6.0 (Broekstraat, Mariakerke, Belgium). After data collection, the data were checked manually for completeness and inconsistencies. The attribute data were expressed as counts and analysed using non-parametric tests. The measurement data are expressed as the mean ± standard deviation. For the normal distribution data, the differences between two groups were analysed using Student's two-sided *t*-test, and differences involving more than two groups were analysed using one-way ANOVA followed by Tukey's *post-hoc* test. For the non-normal distribution data, the likelihood ratio chi-square statistical method was used to assess the differences. The correlation between weight loss and the metabolite levels was analysed with correlation analysis and regression analysis. The level of significance was set at $P < 0.05$.

Results

Baseline clinical characteristics of patients in the training and validation sets

The demographic and clinical data of all the study participants are summarized in Table 1. Forty-six cancer cachexia patients, 22 pre-cachectic patients, 68 weight-stable cancer patients, and 48 healthy controls were included in the training set, while 38 cancer cachexia patients, 11 pre-cachectic patients, 37 weight-stable cancer patients, and 26 healthy controls were included in the validation set. In the training set, all participants were age-matched and sex-matched. The baseline clinical characteristics of patients in the training were showed in Table S1 in the Supplemental Materials. Moreover, there was no significant difference in primary cancer type between the cancer cachexia patients and the weight-stable cancer patients in the training set ($P = 0.59$). However, in the validation set, the cancer cachexia patients were older than the weight-stable cancer patients. The difference among primary tumour types was also significant ($P = 0.02$). Inclusion of different tumour types in the validation set gave insight into the common metabolic profile of cancer cachexia.

Most cancer biomarkers were elevated in the cancer cachexia group relative to the weight-stable cancer group in the training set. The elevated biomarkers included α-fetoprotein, carcinoembryonic antigen, carbohydrate antigen 19–9, carbohydrate antigen 72–4, carbohydrate antigen 12–5, carbohydrate antigen 15–3, carbohydrate antigen 242, carbohydrate antigen 50, cytokeratin 19 fragments, procalcitonin, and interleukin-6. Although interleukin-6 was thought to be a biomarker of cancer cachexia,[26] our results did not indicate that it was a specific biomarker for the diagnosis and classification of cancer cachexia.

The serum biochemical characteristics of the cancer cachexia, pre-cachexia, and weight-stable cancer patients are listed in Table 2. There were no significant differences in total protein or albumin levels. In contrast, low-density lipoprotein and free fatty acids were significantly elevated in the cancer cachexia group, while glucose was decreased. Moreover, the hepatic function and bile metabolism were affected, as indicated by altered levels of direct bilirubin, total bilirubin, total cholesterol, total bile acid, alkaline phosphatase, γ-glutamyltransferase alanine aminotransferase, aspartate aminotransferase, α-hydroxybutyric dehydrogenase, and lactate dehydrogenase. Kidney dysfunction was reflected by elevated serum urea and uric acid in the cancer cachexia patients. Although patients with liver failure were excluded, some patients showed significant variations in relevant biochemical biomarkers, such as direct bilirubin, total bilirubin, total bile acid, alkaline phosphatase, γ-glutamyltransferase, aspartate aminotransferase, α-hydroxybutyric dehydrogenase, and lactate dehydrogenase.

Overall metabolomics analysis of serum samples

Representative NMR spectra of the identified metabolites are shown in Figure 1A. Owing to the overlap in each 1D spectrum, the splitting patterns and coupling constants of each signal could not be recognized. Thus, 2D experiments using J-resolved and HSQC spectra were used for the accurate identification and assignment of metabolites in crowded regions (Figure S1 in the Supplemental Materials). The serum spectra contained high-intensity signals at δ1.18, with a wide peak in the spectrum representing the lipid CH_3 of lipoprotein (VLDL and LDL), as previously reported.[20] In addition, the spectra contained numerous signals from the following small molecules: lactate, alanine, creatine, taurine, glycine, and glucose. The identification, assignment, and source of metabolites are listed in Table S2 in the Supplemental Materials.

Table 2 Serum biochemical characteristics of cancer cachexia patients, cancer patients, and healthy controls in the training set

Item	Cachexia	Pre-cachexia	Cancer
Total protein	60.63 ± 9.40	63.38 ± 14.53	61.18 ± 7.34
Albumin	31.47 ± 5.71	38.15 ± 9.45	34.02 ± 7.99
Pre-albumin	0.15 ± 0.14	0.24 ± 0.14*#	0.13 ± 0.07
Direct bilirubin	38.50 ± 84.32#	32.62 ± 43.33*#	22.99 ± 32.13
Total bilirubin	52.72 ± 102.21*	56.47 ± 81.19*#	36.3 ± 41.84
Total cholesterol	4.55 ± 0.98*	4.24 ± 2.67	4.13 ± 1.28
High-density lipoprotein cholesterol	1.20 ± 0.28	1.56 ± 0.33*#	1.04 ± 0.27
Low-density lipid cholesterol	2.38 ± 1.40	3.08 ± 1.09*#	2.51 ± 1.16
Total bile acid	25.39 ± 49.53*	24.38 ± 28.75*	16.81 ± 18.92
Triglycerides	1.74 ± 1.03*	1.29 ± 0.78#	1.30 ± 0.65
Free fatty acids	0.72 ± 0.35	0.52 ± 0.24*#	0.75 ± 0.21
Glucose	5.95 ± 2.25	5.04 ± 2.94*#	6.06 ± 1.62
Creatinine	70.12 ± 32.74	66.40 ± 37.51	65.67 ± 17.30
Urea	6.41 ± 4.76*	7.81 ± 3.51*#	5.04 ± 1.49
Uric acid	283.54 ± 131.26*	222.27 ± 110.84*#	247.44 ± 90.67
Homocysteine	11.52 ± 6.41*	13.92 ± 5.82*#	12.51 ± 7.60
Alanine aminotransferase	34.26 ± 45.35*	22.71 ± 43.67#	25.00 ± 18.08
Aspartate aminotransferase	54.29 ± 84.49*	43.97 ± 83.92*#	32.78 ± 19.34
Alkaline phosphatase	224.84 ± 231.31	162.84 ± 110.29*#	242.65 ± 269.46
α-Hydroxybutyric dehydrogenase	260.30 ± 292.64*	200.15 ± 142.76*#	170.13 ± 35.49
γ-Glutamyltransferase	167.15 ± 266.37*	116.75 ± 164.22#	119.73 ± 160.01
Lactate dehydrogenase	322.72 ± 410.64*	223.20 ± 210.20*#	209.56 ± 46.02

*Significant difference from cancer patients.
#Significant difference from cachexia patients

Although the overall signals were similar among the four groups, there were seemingly specific signals in each group. The statistical evaluation by PCA (Principal Component Analysis) showed separation of healthy control from the other three groups. The widespread of the samples in the PCA was caused by different levels of metabolic manifestations within subjects and/or by the date of subsequent sampling. To exclude possible confounding variables that were not related to the group differences and to evaluate the statistical significance of those signals, OPLS were applied (Figure 2A). The result was encouraging as the discrimination model could differentiate the healthy control, tumour, and cachexia groups. The multiple testing results of the identified metabolites are listed in Table S3 in the Supplemental Materials. The heat map of samples and metabolites were analysed with Metaboanalyst 3.0. The distance measure was Euclidean, and the clustering algorithm was average. The samples clustered according to their natural affiliation as four groups (Figure S2 in the Supplemental Materials). Although the distributions of pre-cachexia overlapped with tumour and cachexia samples, the models showed high cross-validation predictability and goodness-of-fit values, with R^2Y (cum) = 0.738 andQ^2 (cum) = 0.697, indicating reliable differentiation between the groups.[27]

Typical cachexia-related serum metabolites

To identify distinct biomarkers that may be associated with cancer cachexia among thousands of variables, a pairwise comparison was conducted between the cancer cachexia group and weight-stable cancer patients (Figure 2B). The model for classification of these groups obtained satisfactory validation, with R^2Y (cum) = 0.968 and Q^2 (cum) = 0.907. To identify the most reliable discriminating variables (those that were highly diagnostic for group separation), a visualized S-plot (Figure 2C) was employed, with p1 and p1 (corr) set as $> \pm 0.05$. Using this method together with the VIP from the OPLS-DA model described above, a total of 15 metabolites with VIP > 1 were selected, including elevated levels of pyruvate, lysine, succinate, choline, isoleucine, 5-hydroxylysine, tyrosine, creatine, myo-inositol, glycocholate, 1-methylhistidine, and glucose and decreased levels of lactate, fatty acid, leucine, n-acetylglutamate, glutamate, carnitine, citrate, 4-hydroxyproline, malate, and alanine.

To reduce the false-positive risk in the metabolite selection procedure, another pairwise comparisons between the cancer cachexia and normal control groups were conducted. The score plot (Figure 2D) also showed clear separation of cachexia and normal control groups, with R^2Y (cum) = 0.986 and Q^2 (cum) = 0.970. The visualized S-plot (Figure 2E) and the variables with high VIP indicated 21 differential metabolites, including elevated levels of lysine, citrulline, cis-aconitate, methionine, succinate, pyruvate, glutamate, n-acetylcysteine, alanine, 1-methylhistidine, n-acetylglutamate, anserine, 5-hydroxylysine, creatine, tyrosine, myo-inositol, glycocholate, 2-hydroxyisovalerate, and glucose and decreased levels of choline, carnitine, fatty acids, leucine, citrate, 4-hydroxyproline, and valine.

Pre-cachexia-related serum metabolites

To reveal pre-cachexia-related serum metabolites, pairwise comparisons between the cancer cachexia and pre-cachexia

Figure 1 Typical 600 MHz ^{1}H-NMR spectra of (A) sera and (B) urine from cancer cachexia patients, pre-cachectic patients, weight-stable cancer patients, and healthy controls. The metabolites are assigned and marked.

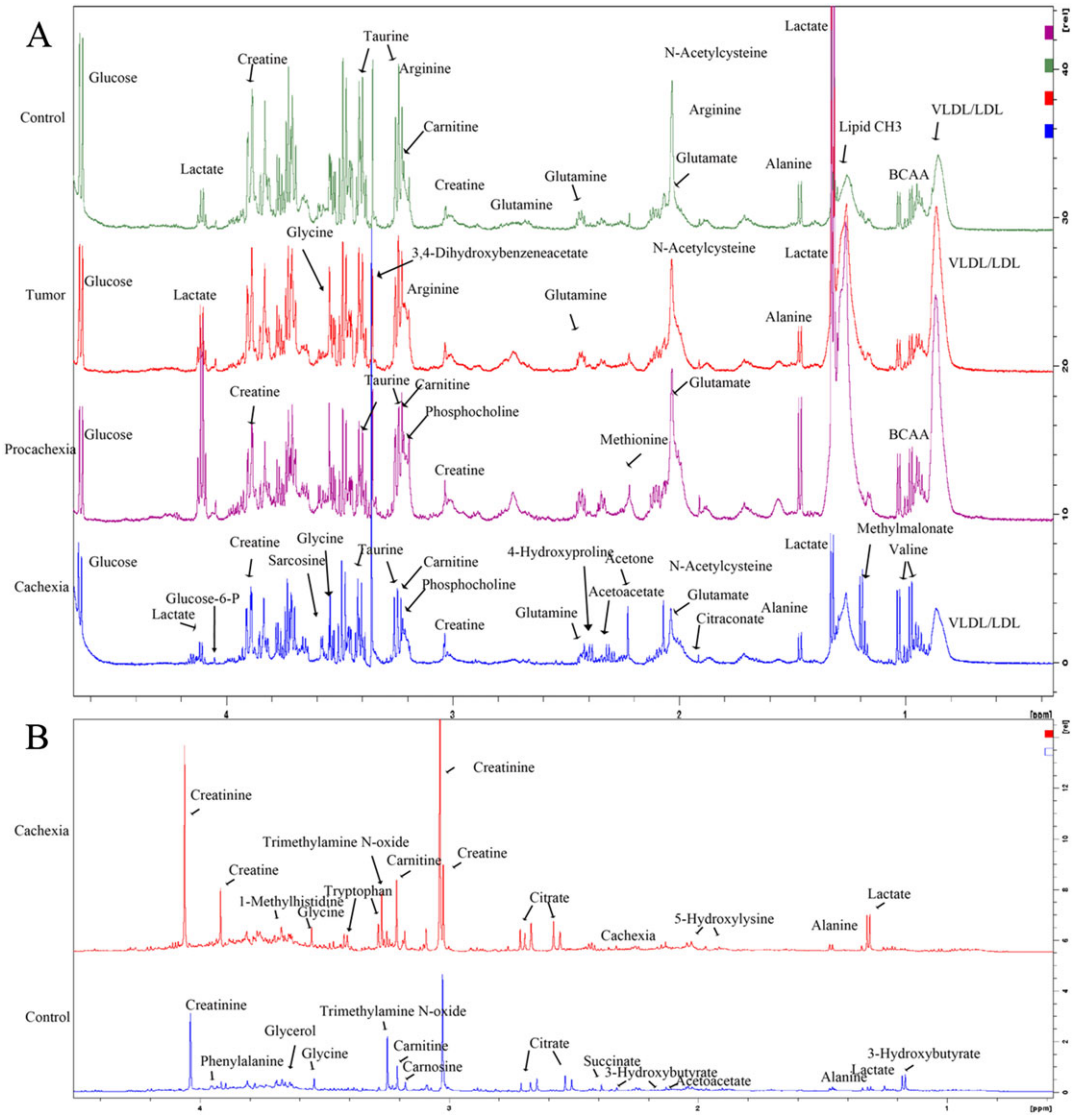

groups were conducted. The score plot (Figure 3A) of the OPLS-DA model showed clear separation, with R2Y (cum) = 0.978 and Q2 (cum) = 0.882. The S-plot (Figure 3B) indicated the changed metabolites. Compared with pre-cachexia, cachexia showed increased glycocholate, myo-inositol, creatine, 1-methylhistidine, 5-hydroxylysine, tyrosine, and succinate and decreased lactate, fatty acids, leucine, N-acetylglutamate, glutamate, citrate, carnitine, methylmalonate, 3-hydroxybutyrate, malate, N-acetylcysteine, alanine, glutamine, methionine, 4-hydroxyproline, glycine, and threonine.

To reveal pre-cachexia-related serum metabolites, two other pairwise comparisons were conducted. The score plot (Figure 3C) of the OPLS-DA model from pairwise comparison between pre-cachectic patients and weight-stable tumour patients showed partial separation, with R2Y (cum) = 0.647 and Q2 (cum) = 0.570. The S-plot (Figure 3 D) and the variables with high VIP revealed the metabolic effect of pre-cachexia, including elevated levels of lactate, tyrosine, N-acetylglutamate, N-acetylcysteine, glutamate, 5-hydroxylysine, glutamine, methionine, alanine, myo-inositol, creatine, carnitine, leucine, glycine, isoleucine, anserine, threonine, malate, choline, fatty acid, glycocholate, pyruvate, lysine, and citrate and decreased levels of glucose, 3-hydroxybutyrate, cis-aconitate, 4-hydroxyproline, methylmalonate, acetone, 1-methylhistidine, and taurine. The score plot (Figure 3E) of the OPLS-DA model from the pairwise comparison between pre-cachectic patients and weight-stable healthy controls revealed clear separation, with R2Y (cum) = 0.972 and Q2 (cum) = 0.942. The S-plot

DOI: 10.1002/jcsm.12246

Figure 2 Overall serum metabolic profile of four groups and the metabolic profiles associated with cancer cachexia. The OPLS-DA score plot of the four groups revealed the clustering of samples in the training set (A). To identify the unique metabolites associated with cancer cachexia, two comparison analyses were conducted. OPLS-DA score plots (B, D) showed strong clustering of each group, with little difference within the subjects, while an S-plot (C, E) identified the metabolites. The metabolites with p1 and p1 (corr) $>$ ± 0.05 were marked by the first component in the S-plots. Comparisons between cancer cachexia and cancer patients (B, C) and between cancer cachexia patients and healthy controls (D, E).

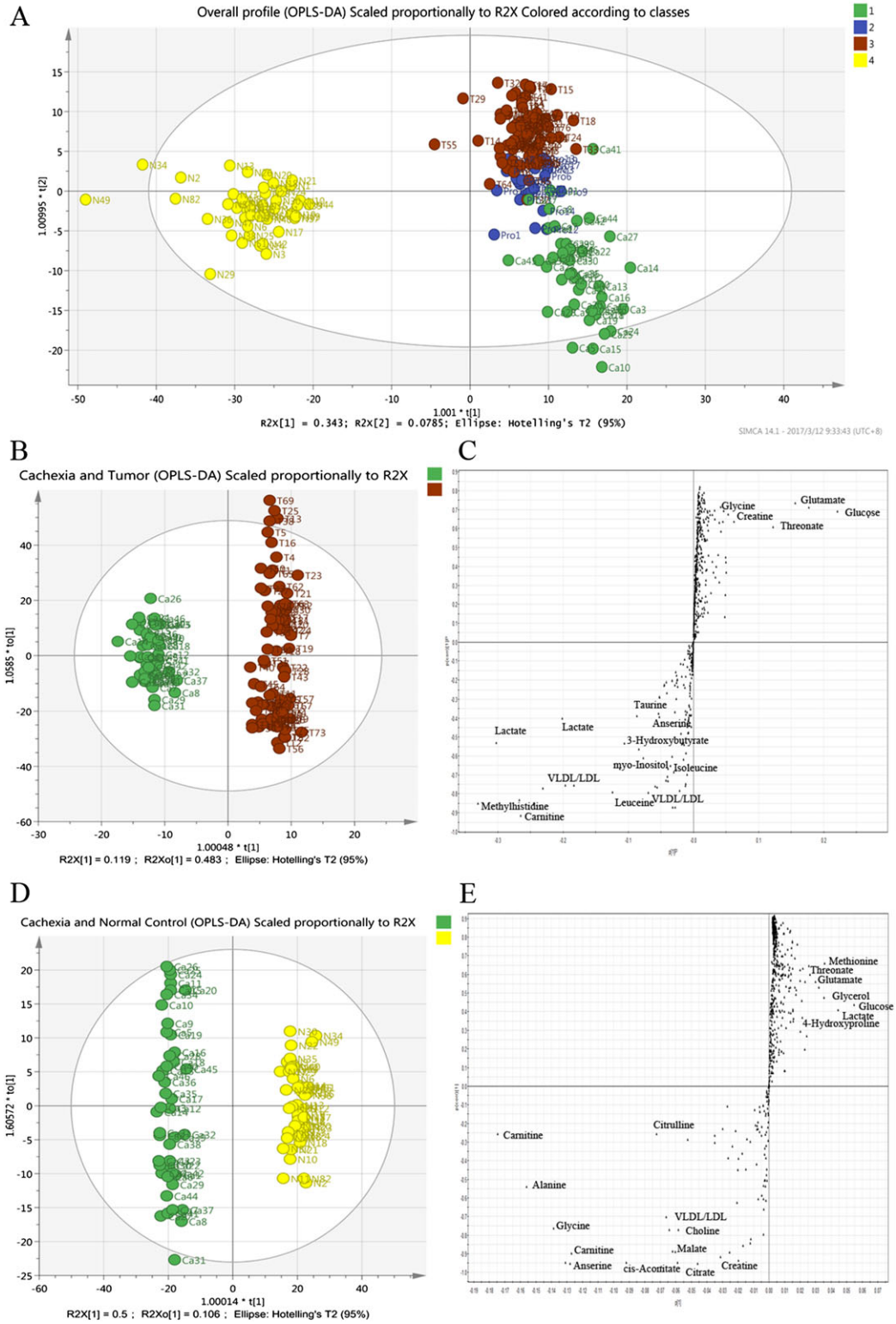

DOI: 10.1002/jcsm.12246

Figure 3 Serum metabolic profiles associated with pre-cachexia. OPLS-DA score plots (A, C, E) showed clustering, while an S-plot (B, D, F) identified the metabolites. Comparisons between cancer cachexia and pre-cachectic patients (A, B) between pre-cachexia and cancer patients (C, D) and between pre-cachectic patients and healthy controls (E, F) revealed metabolites associated with pre-cachexia.

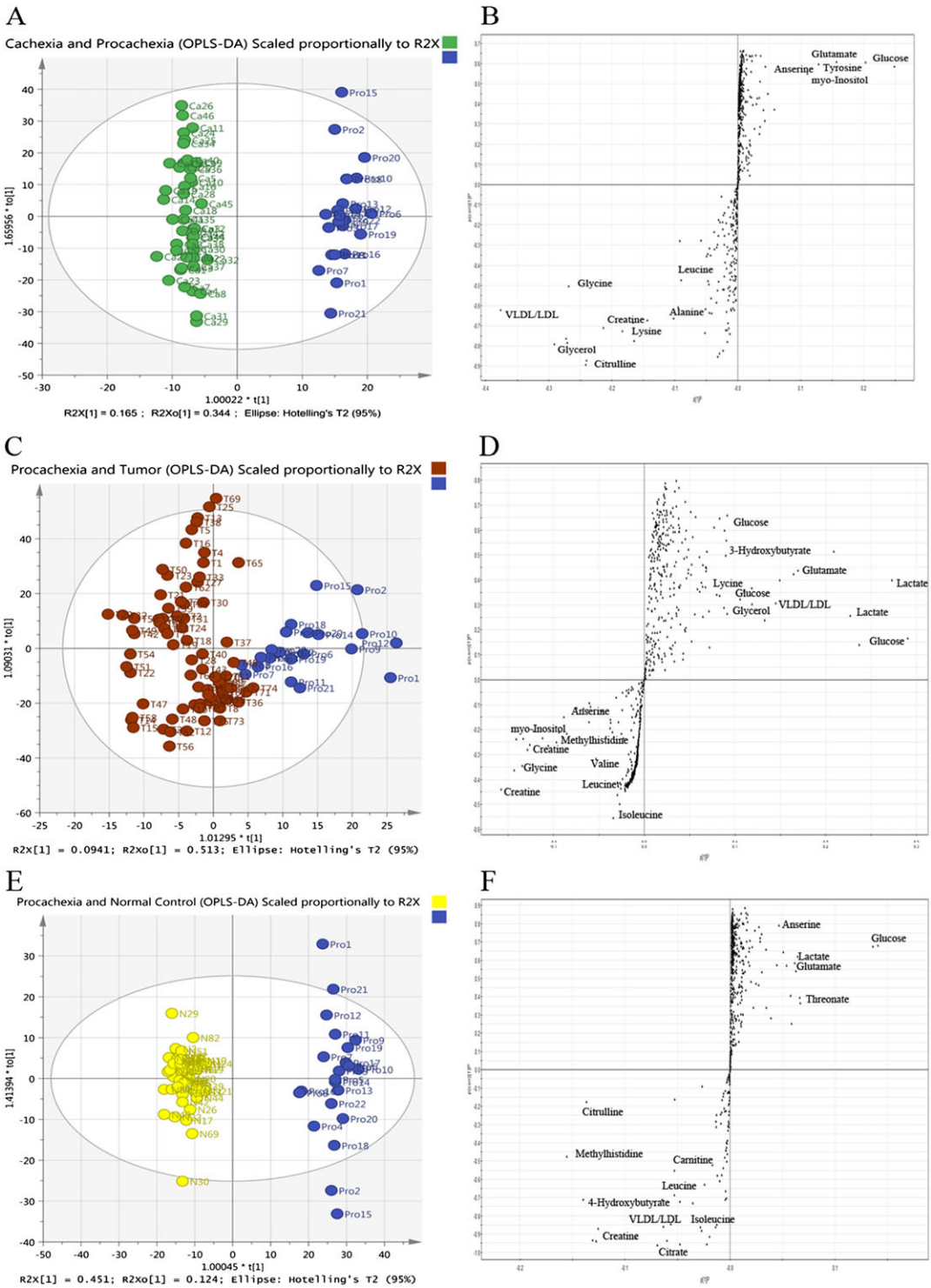

(Figure 3F) and the variables with high VIP revealed the metabolic effect of pre-cachexia, including elevated levels of lactate, leucine, fatty acid, glutamate, N-acetylglutamate, 1-methylhistidine, alanine, N-acetylcysteine, methylmalonate, anserine, tyrosine, myo-inositol, methionine, 5-hydroxylysine, taurine, glutamine, citrate, malate, pyruvate,

DOI: 10.1002/jcsm.12246

3-hydroxybutyrate, succinate, creatine, glycocholate, acetone, cis-aconitate, threonine, and citrulline and decreased levels of 4-hydroxyproline, glycine, carnitine, glucose, and choline.

Cancer-related serum metabolites

To reduce the interference from cancer, pairwise comparison between cancer patients and weight-stable healthy controls were conducted. The R^2Y (cum) = 0.970 and Q^2 (cum) = 0.955 of the OPLS-DA model were close to 1, indicating an excellent model. The score plot (Figure 4A) and S-plot (Figure 4B) revealed the metabolic effect of tumours, including elevated levels of glycocholate, citrulline, succinate, cis-aconitate, malate, glutamine, pyruvate, methionine, citrate, tyrosine, myo-inositol, acetone, valine, isoleucine, n-acetylcysteine, anserine, alanine, methylmalonate, taurine, glutamate, n-acetylglutamate, fatty acid, leucine, lactate, and 1-methylhistidine and decreased levels of choline, glucose, carnitine, and glycine. These metabolites revealed a highly unique metabolic cancer phenotype characterized by glycolysis, the mitochondrial citric acid cycle, choline, and altered fatty acid metabolism.

Typical cachexia-related urine metabolites

The urine ^{1}H-NMR spectrum and metabolite biomarkers are shown in Figure 1B. The differences between cancer cachexia patients and controls were also assessed using a PCA model, which showed clear separation. To exclude unfit variables from the candidate list, OPLS-DA was applied (Figure 5A). The first two principal components were able to differentiate cancer cachexia patients from the control groups. The potentially significant-related metabolites were identified following the same procedure that was used for serum metabolites. By combining the variables with high VIP with the S-Plot (Figure 5B), 22 metabolites were finally identified as potential biomarkers, including increased levels of 3-hydroxybutyrate, phenylalanine, 1-methylhistidine, glycine, glycerol, N-acetylglutamate, acetoacetate, tryptophan, creatine, and 3-aminobutyrate and decreased levels of uridine, fatty acids, isoleucine, leucine, methylmalonate, serine, carnosine, valine, anserine, 5-hydroxylysine, and phenyl acetate. As listed in Supplemental Table S2, 12 metabolites are found both in serum and urine samples, 3-hydroxybutyrate, 1-methylhistidine, 5-hydroxylysine, anserine, citrulline, creatine, glycocholate, methylmalonate, glycine, leucine, isoleucine, and valine. The overlapping amino acids and their intermediate metabolites might reflect a common metabolic reprogramming.

Metabolite profiling and cancer cachexia-related pathways

The altered metabolites in serum and urine were pooled for analysis, giving a total of 45 metabolites. Correlation analysis was employed to show the relationships among the metabolites. A heat map of the correlation analysis revealed that the metabolites could be divided into four categories (Figure S3 of the Supplemental Materials). All 45 identified metabolites were analysed using Metaboanalyst 3.0. The concentrations of the examined metabolites in the four groups are shown in Figure S4 of the Supplemental Materials. The pathway analysis showed the detailed impacts of cancer cachexia-related alterations in metabolic networks (Figure 6). The most influential metabolic pathway had a pathway impact >0.05 and log

Figure 4 Serum metabolomics between cancer patients and healthy controls (A, B) revealed metabolites associated with cancer. OPLS-DA score plots of cancer patients and healthy controls (A) showed clear distinction. S-plots revealed metabolites with p1 and p1 (corr) > ± 0.05 from the first component (B).

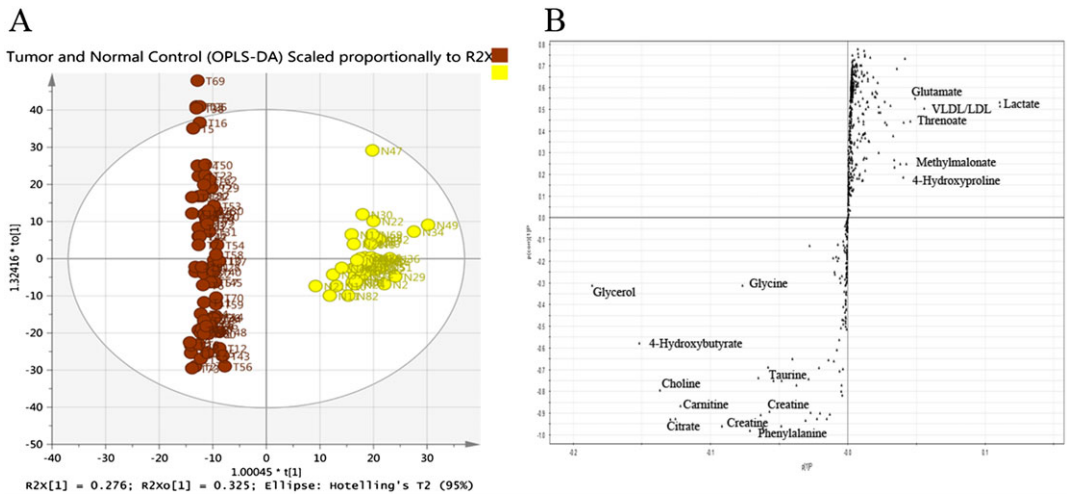

DOI: 10.1002/jcsm.12246

Figure 5 Urine metabolomics analysis identified metabolites associated with cancer cachexia. OPLS-DA score plots of cancer cachexia patients and healthy controls (A) showed clear distinction. S-plots revealed metabolites with p1 and p1 (corr) > ± 0.05 from the first component (B).

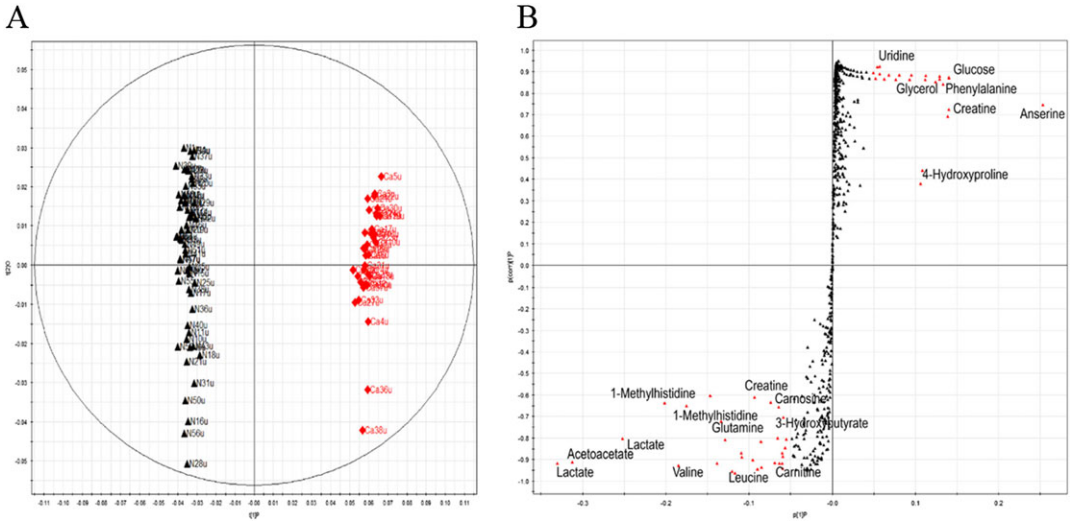

(p) > 20. Eighteen metabolic pathways were defined as disturbed in the plasma and urine profiles of cancer cachexia patients, including the synthesis and degradation of valine, leucine and isoleucine, lysine, and ketone bodies; the citrate cycle; the metabolism of glycine, serine, threonine, glutamine, glutamate, taurine, pyruvate, alanine, aspartate, glutamate, glycerolipids, phenylalanine, butanoate, glycerophospholipids, inositol phosphate, arginine, proline, cysteine, and methionine; and aminoacyl-tRNA biosynthesis.

Figure 6 Cachexia triggers metabolic pathway reprogramming. Plots depict the computed metabolic pathways as a function of −log(p) (*y*-axis) and the pathway impacts of the key metabolites (*x*-axis) that differed between the cancer cachexia and non-cachexia groups.

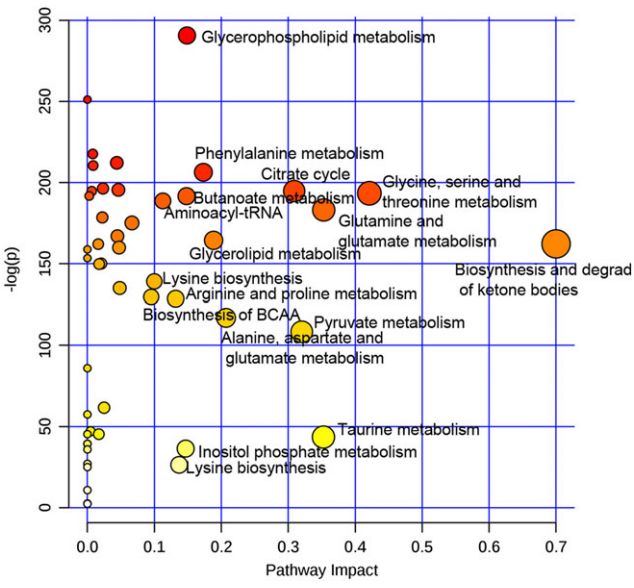

Selection of biomarkers and validation of the diagnostic model

Using the metabolic profile of cancer cachexia with the 45 differential metabolites, it was difficult to establish a diagnostic model to predict the presence of cachexia in cancer patients. Random forest analysis was executed to estimate the importance of each metabolite in the training dataset.[19] As presented in Figure 7A, we found the15 metabolites clearly achieved higher significance than the other metabolites. To screen cachexia, we use a logistic regression to establish a diagnostic model based on three metabolites. The diagnostic regression equation was as follows: Logit (P) = −400.53 − 481.88 * log (Carnosine) −239.02 * log (Leucine) + 383.92 * log (Phenyl acetate). The corresponding ROC curve had an AUC of 0.991 (95% CI: 0.938–1.000) with a Youden index J of 0.895 (Figure 7B). To validate the results, we analysed the association of the samples in the validation datasets. Only six samples in the validation set were ambiguous, and the accuracy was 94.64%. It should be noted that the AUC of the combined diagnostic model was better than that for each metabolite, indicating that the diagnostic equation based on three metabolites yielded the highest AUC value and could significantly improve the diagnostic performance with respect to cancer cachexia.

Discussion

In this study, we performed a ^{1}H-NMR-based metabolomics analysis to reveal the metabolic profile of cancer cachexia and to establish a diagnostic model. Overall, 84 cancer cachexia patients, 33 pre-cachectic patients, 105 cancer

DOI: 10.1002/jcsm.12246

Figure 7 Random forest analysis revealed the 15 most important metabolites (A). ROC curves of the diagnostic metabolites and combined equation in the validation sets (B).

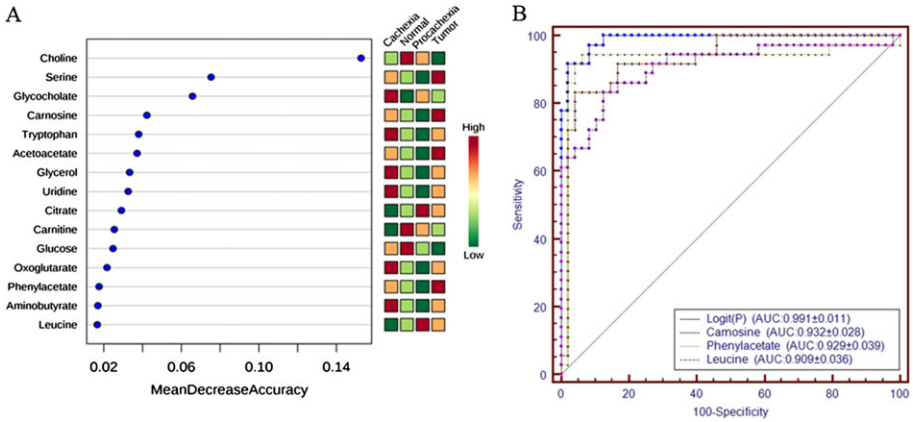

patients, and 74 healthy controls were included in the training and validation sets. Metabolomics analysis revealed clear separation based on metabolic profiling. To predict the presence of cachexia, a diagnostic model was established based on three metabolites, namely, carnosine, leucine, and phenyl acetate, with high accuracy and confirmation by the validation set (94.64% by diagnostic feature).

In the metabolic profile, decreased levels of glucose and elevated levels of lactate were observed in the cachexia patients' sera, consistent with previous reports.[17,18] Enhanced glucose metabolism in cancer has been associated with glycolysis, leading to greater pyruvate and lactate formation via non-oxidative pathways. However, the disruption of glucose metabolism and its intermediate metabolites is similar to certain characteristics of cancer cell metabolism, and its specificity to cancer cachexia is limited. Comparative analysis and metabolic pathway analysis were employed to identify distinct metabolites and pathway changes of cancer cachexia. A total of 45 metabolites and 18 metabolic pathways were found to be associated with cancer cachexia. Because the metabolites were collinear, we employed random forest and logistic regression analyses to establish a diagnostic model. In the selection of biomarkers and validation of the diagnostic model, random forest analysis identified the 15 highly discriminating metabolites among 45 metabolites; logistic regression analysis revealed a distinct diagnostic equation based on 3 metabolites, and ROC analysis elucidated that the diagnostic performance of the equation was higher than each metabolite.

Carnosine levels were decreased in cancer patients and elevated in cachexia patients. ROC analysis was conducted and showed an AUC of 0.932, implying high specificity and sensitivity. Carnosine is a dipeptide of histidine and alanine that is present at high concentrations in skeletal muscle and brain tissue.[28] Previous studies showed that carnosine supplementation can regulate brain function in some patients and elevate plasma corticosterone concentrations via the hypothalamic-pituitary-adrenal axis.[29] Recent research has demonstrated that carnosine has the potential to suppress the multiple biochemical changes of protein oxidation, glycation, and cross-linking.[30] Low carnosine dipeptidase-1 levels have also been associated with poor cancer prognosis, including weight loss, malnutrition, lipid breakdown, low circulating albumin, IGF1 levels, and poor quality of life in gastrointestinal cancer.[31] These results, together with other recently published data, indicate that carnosine contributes to body-weight regulation.[22]

Leucine is a branched-chain amino acid (BCAA). BCAAs such as valine, isoleucine, and leucine are essential amino acids whose carbon structures are marked by a branch point. They are essential to human life and are particularly involved in nutrient and energy metabolism. Consistent evidence has shown that BCAAs are not only important energy substrates but also act as precursors that improve nitrogen retention and protein synthesis.[32] Research has also shown that nutritional leucine supplementation can stimulate muscle protein anabolism, inhibit catabolism, and modulate glucose homeostasis.[33,34] Infusion of leucine can promote the synthesis of glutamine and alanine. Moreover, BCAAs are primarily catabolized in skeletal muscle, and they have been proposed for the treatment of catabolic disease states involving skeletal muscle wasting.[35,36] Despite their structural similarities, the branched-chain amino acids belong to different metabolic pathways, with leucine going solely to fats, valine solely to carbohydrates, and isoleucine to both. In our study, the changes in valine and isoleucine levels were different from those in leucine levels. Our correlation analysis of metabolites also revealed different effects on these three amino acids. Leucine was elevated in cancer patients and decreased in cachexia patients. The AUC in the ROC analysis was 0.909, suggesting a high-predictive value of leucine for the diagnosis and classification of cancer cachexia.

Phenyl acetate was found to be decreased in cancer patients and increased in cachexia. Phenyl acetate can be

DOI: 10.1002/jcsm.12246

converted to phenylpyruvate by transamination or may be further conjugated with glutamine to form phenylacetyl glutamine. It is produced endogenously by monoamine oxidase as the metabolite of 2-phenylethylamine, which may modulate central adrenergic functions.[37] Previous studies postulated that urine phenyl acetate may be a biomarker for depression.[38] The demand for nutrients leads to the depletion of phenyl acetate in cancer, and cancer cachexia results in the accumulation of urine phenyl acetate. The AUC in the ROC analysis was 0.929. These results demonstrate the differences in the metabolite profiles of cancer patients and cachexia patients.

To validate the significance of metabolites as potential cancer cachexia biomarkers, logistic regression analysis was employed to generate an optimal model using the three metabolites. The diagnostic model had an AUC of 0.991 in the corresponding ROC curve, with high specificity and sensitivity. Currently, cachexia is diagnosed based on objective measures of clinical symptoms, and its diagnosis depends on a history of weight loss.[39] This diagnostic criterion lags behind disease progression and has limited utility for the early diagnosis of cancer cachexia.[4] The emergence of metabolomics has immense potential for the early diagnosis and understanding of the pathogenesis of cancer cachexia. Endogenous metabolites are the end products of physiological processes, and many key metabolites may function intracellularly as modulators by regulating the activity of enzymes, which are considered responsible for the pathophysiological process. NMR-based metabolomics is an unbiased method to distinguish metabolites. Thus, high resolution ^{1}H-NMR-based metabolomics was employed to reveal the metabolic profiles in the present study. When we compared our study with the results from Di Gangi *et al*.,[19] 17 common metabolites were found, including alanine, arginine, asparagine, creatinine, glucose, glutamine, glycine, histidine, isoleucine, leucine, lysine, phenylalanine, taurine, threonine, tryptophan, tyrosine, and valine. While NMR-based metabolomics and LC-MS-based metabolomics can measure different metabolites, these methods identified common changes in amino acid and intermediate metabolites, underscoring the robustness of the data.

It should be noted that our previous study revealed changes in 13 metabolites from the intact muscle gastrocnemius and 43 metabolites from the serum in our murine dynamic cancer cachexia model.[20] The common changes in metabolites between murine and human samples included 2-oxoglutarate, 3-hydroxybutyrate, 3-methylhistidine, acetoacetate, aconitate, alanine, anserine, carnitine, carnosine, choline, cis-aconitate, citrate, citrulline, creatine, glucose, glutamate, glutamine, glycerol, glycine, isocitrate, lactate, leucine, lysine, malate, methionine, phenyl acetate, phenylalanine, pyruvate, serine, succinate, taurine, taurine, threonate, valine, and VLDL/LDL. Another 10 metabolites were not found to be changed in the murine cachexia model, which might be related to the fact that species, tumour types, and environment were different. After excluding the collinear metabolites, we could establish a simple and feasible diagnostic model. A longitudinal research design will be convincing to verify the results because longitudinal design can help to show dynamic change trends of metabolites over time, in parallel with the severity of cachexia. It was interesting that when we analysed the correlation between the severity of cachexia (determined by % weight loss) and the metabolite levels calculated from the model, the correlation coefficient was 0.563 and significance level was less than 0.05. These indicated the levels of metabolites were correlated with the severity of cachexia.

In conclusion, this study reports a metabolomics analysis of serum and urine from cancer cachexia patients. Forty-five distinguishable metabolites were identified, and 18 metabolic pathways were found to change in association with cachexia. To select the biomarkers and validate the diagnostic model, random forest identified the 15 highly discriminating metabolites among 45 metabolites, and logistic regression revealed a distinct diagnostic equation based on three metabolites. ROC analysis demonstrated that the diagnostic performance of the equation was higher than that for each metabolite, and the AUC of the diagnostic model was 0.991. The accuracy was 94.64% in the validation set, and these results indicated a feasible diagnostic approach for identifying at-risk populations through the detection of metabolites. Therefore, the signature model based on the three metabolites could improve the diagnostic performance with respect to cachexia.

Acknowledgements

The present study was supported by grants from the Natural Science Foundation of China (No. 81503155). The authors certify that they comply with the ethical guidelines for authorship and publishing of the Journal of Cachexia, Sarcopenia and Muscle.[40]

Online supplementary material

Additional Supporting Information may be found online in the supporting information tab for this article.

Fig. S1. The metabolites are assigned and marked. The overlapping peaks were identified by 2D J-resolved (A) and HSQC (B) spectra.Figure S2. The heat map of samples and metabolites analysed with Metaboanalyst 3.0. The distance measure was Euclidean, and the clustering algorithm was average. The samples clustered as four groups (cachexia, pre-cachexia, body weight stable cancer groups and healthy control)

according to their natural affiliation.Figure S3. The heat map of correlation analysis analysed with Metaboanalyst 3.0. All the 45 metabolites clustered as two subgroups.Figure S4. The concentration of the examined metabolites in the four groups.

Table S1. Baseline clinical characteristics of patients in the training setsTable S2. The identification, assignment, sample source of metabolites in samples and their related metabolic pathways.Table S3. The multiple testing results of the identified metabolites.

Conflict of interest

None declared.

Authors' contributions

Conception and design were performed by Yang Quan-Jun and Guo Cheng. Sample selection and collection were carried out by Zhang Jiang-Rong, Hao Juan and Li Bin.

NMR experiment was performed by Yang Gen-Jin. Metabolites identification was carried out by Yang Quan-Jun, Yang Gen-Jin, Huang Jin-Lu, and Gan Run. Data analysis was performed by Yang Quan-Jun, Li Jie, Lu Jin, Han Yong-Long, and Guo Cheng. Administrative, technical, and material support were carried out by Wan Li-Li, Huo Yan, and Han Yong-Long. Manuscript preparation was performed by Yang Quan-Jun, Zhang Jiang-Rong, and Guo Cheng. Study supervision was carried out by Guo Cheng and Huo Yan.

References

1. Temel JS et al. Anamorelin in patients with non-small-cell lung cancer and cachexia (ROMANA 1 and ROMANA 2): results from two randomised, double-blind, phase 3 trials. *Lancet Oncol* 2016;**17**:519–531.
2. Fearon KC. Cancer cachexia and fat–muscle physiology. *New England Journal of Medicine* 2011;**365**:565–567.
3. Molfino A et al. Novel therapeutic options for cachexia and sarcopenia. *Expert Opin Biol Ther* 2016;1–6.
4. Drescher C et al. Loss of muscle mass: current developments in cachexia and sarcopenia focused on biomarkers and treatment. *J Cachexia Sarcopenia Muscle* 2015;**6**:303–311.
5. Kalantar-Zadeh K et al. Why cachexia kills: examining the causality of poor outcomes in wasting conditions. *J Cachexia Sarcopenia Muscle* 2013;**4**:89–94.
6. Quan-Jun Y et al. Selumetinib attenuates skeletal muscle wasting in murine cachexia model through ERK inhibition and AKT activation. *Mol Cancer Ther* 2017; **16**:334–343.
7. Garcia JM et al. Anamorelin for patients with cancer cachexia: an integrated analysis of two phase 2, randomised, placebo-controlled, double-blind trials. *Lancet Oncol* 2015;**16**:108–116.
8. Zhou X et al. Reversal of cancer cachexia and muscle wasting by ActRIIB antagonism leads to prolonged survival. *Cell* 2010;**142**: 531–543.
9. Santarpia L, Contaldo F, Pasanisi F. Nutritional screening and early treatment of malnutrition in cancer patients. *J Cachexia Sarcopenia Muscle* 2011;**2**:27–35.
10. Fearon K et al. Definition and classification of cancer cachexia: an international consensus. *Lancet Oncol* 2011;**12**:489–495.
11. Lucia S et al. Cancer cachexia: from molecular mechanisms to patient's care. *Crit Rev Oncog* 2012;**17**:315–321.
12. Petruzzelli M, Wagner EF. Mechanisms of metabolic dysfunction in cancer-associated cachexia. *Genes Dev* 2016;**30**:489–501.
13. Honors MA, Kinzig KP. The role of insulin resistance in the development of muscle wasting during cancer cachexia. *J Cachexia Sarcopenia Muscle* 2012;**3**:5–11.
14. Sah RP et al. New insights into pancreatic cancer-induced paraneoplastic diabetes. *Nat Rev Gastroenterol Hepatol* 2013.
15. Braun TP et al. Cancer- and endotoxin-induced cachexia require intact glucocorticoid signaling in skeletal muscle. *FASEB J* 2013;**27**:3572–3582.
16. Seelaender MC, Batista ML. Adipose tissue inflammation and cancer cachexia: the role of steroid hormones. *Horm Mol Biol Clin Investig* 2014;**17**:5–12.
17. Der-Torossian H et al. Cancer cachexia's metabolic signature in a murine model confirms a distinct entity. *Metabolomics* 2013;**9**:730–739.
18. O'Connell TM et al. Metabolomic analysis of cancer cachexia reveals distinct lipid and glucose alterations. *Metabolomics* 2008;**4**:216–225.
19. Di Gangi IM et al. Metabolomic profile in pancreatic cancer patients: a consensus-based approach to identify highly discriminating metabolites. *Oncotarget* 2016;**7**: 5815–5829.
20. QuanJun Y et al. Integrated analysis of serum and intact muscle metabonomics identify metabolic profiles of cancer cachexia in a dynamic mouse model. *RSC Adv* 2015;**5**:92438–92448.
21. Quanjun Y et al. Serum metabolic profiles reveal the effect of formoterol on cachexia in tumor-bearing mice. *Mol Biosyst* 2013;**9**:3015–3025.
22. Quan-Jun Y et al. NMR-based metabolomics reveals distinct pathways mediated by curcumin in cachexia mice bearing CT26 tumor. *RSC Adv* 2015;**5**:11766–11775.
23. Beckonert O et al. Metabolic profiling, metabolomic and metabonomic procedures for NMR spectroscopy of urine, plasma, serum and tissue extracts. *Nat Protoc* 2007;**2**:2692–2703.
24. QuanJun Y et al. Protective effects of dexrazoxane against doxorubicin-induced cardiotoxicity: a metabolomic study. *PLoS One* 2017;**12**: e0169567.
25. Quan-Jun Y et al. Distinct metabolic profile of inhaled budesonide and salbutamol in asthmatic children during acute exacerbation. *Basic Clin Pharmacol Toxicol* 2017; **120**:303–311.
26. Scheede-Bergdahl C et al. Is IL-6 the best pro-inflammatory biomarker of clinical outcomes of cancer cachexia? *Clin Nutr* 2012;**31**:85–88.
27. Aberg KM, Alm E, Torgrip RJ. The correspondence problem for metabonomics datasets. *Anal Bioanal Chem* 2009;**394**: 151–162.
28. Dunnett M, Harris R. Carnosine and taurine contents of type I, IIA and IIB fibres in the middle gluteal muscle. *Equine Vet J* 1995;**27**:214–217.
29. Bae O-N et al. Safety and efficacy evaluation of carnosine, an endogenous neuroprotective agent for ischemic stroke. *Stroke* 2013;**44**:205–212.
30. Letzien U et al. The antineoplastic effect of carnosine is accompanied by induction of PDK4 and can be mimicked by L-histidine. *Amino Acids* 2014;**46**:1009–1019.
31. Arner P et al. Circulating carnosine dipeptidase 1 associates with weight loss and poor prognosis in gastrointestinal cancer. *PLoS One* 2015;**10**: e0123566.
32. Li F et al. Leucine nutrition in animals and humans: mTOR signaling and beyond. *Amino Acids* 2011;**41**:1185–1193.
33. van Norren K et al. Dietary supplementation with a specific combination of high protein, leucine, and fish oil improves muscle function and daily activity in tumour-

bearing cachectic mice. *Br J Cancer* 2009; **100**:713–722.
34. Caperuto EC et al. Beta-hydoxy-beta-methylbutyrate supplementation affects Walker 256 tumor-bearing rats in a time-dependent manner. *Clin Nutr* 2007;**26**: 117–122.
35. Chen Y et al. Leucine-stimulated mTOR signaling is partly attenuated in skeletal muscle of chronically uremic rats. *Am J Physiol Endocrinol Metab* 2011;**301**: E873–E881.
36. Giron MD et al. Conversion of leucine to beta-hydroxy-beta-methylbutyrate by alpha-keto isocaproate dioxygenase is required for a potent stimulation of protein synthesis in L6 rat myotubes. *J Cachexia Sarcopenia Muscle* 2016;**7**:68–78.
37. Mosnaim AD, Hudzik T, Wolf ME. Behavioral effects of β-phenylethylamine and various monomethylated and monohalogenated analogs in mice are mediated by catecholaminergic mechanisms. *Am J Ther* 2015;**22**:412–422.
38. Wijburg FA and Nassogne M-C, *Disorders of the urea cycle and related enzymes*, in *inborn metabolic diseases*. 2012, Springer. p. 297-310.
39. Martins T et al. Biomarkers for cardiac cachexia: reality or utopia. *Clin Chim Acta* 2014;**436**:323–328.
40. von Haehling S, Morley JE, Coats AJS, Anker SD. Ethical guidelines for publishing in the Journal of Cachexia, Sarcopenia and Muscle: update 2015. *J Cachexia Sarcopenia Muscle* 2015;**6**:315–316.